Webster, J.M., Ravelo, A.C., Grant, H.L.J., and the Expedition 389 Scientists
Proceedings of the International Ocean Discovery Program Volume 389
publications.iodp.org

Site M0104[1]

J.M. Webster, A.C. Ravelo, H.L.J. Grant, M. Rydzy, M. Stewart, N. Allison, R. Asami, B. Boston, J.C. Braga, L. Brenner, X. Chen, P. Chutcharavan, A. Dutton, T. Felis, N. Fukuyo, E. Gischler, S. Greve, A. Hagen, Y. Hamon, E. Hathorne, M. Humblet, S. Jorry, P. Khanna, E. Le Ber, H. McGregor, R. Mortlock, T. Nohl, D. Potts, A. Prohaska, N. Prouty, W. Renema, K.H. Rubin, H. Westphal, and Y. Yokoyama[2]

[1] Webster, J.M., Ravelo, A.C., Grant, H.L.J., Rydzy, M., Stewart, M., Allison, N., Asami, R., Boston, B., Braga, J.C., Brenner, L., Chen, X., Chutcharavan, P., Dutton, A., Felis, T., Fukuyo, N., Gischler, E., Greve, S., Hagen, A., Hamon, Y., Hathorne, E., Humblet, M., Jorry, S., Khanna, P., Le Ber, E., McGregor, H., Mortlock, R., Nohl, T., Potts, D., Prohaska, A., Prouty, N., Renema, W., Rubin, K.H., Westphal, H., and Yokoyama, Y., 2025. Site M0104. In Webster, J.M., Ravelo, A.C., Grant, H.L.J., and the Expedition 389 Scientists, Hawaiian Drowned Reefs. Proceedings of the International Ocean Discovery Program, 389: College Station, TX (International Ocean Discovery Program). https://doi.org/10.14379/iodp.proc.389.111.2025

[2] **Expedition 389 Scientists' affiliations.**

Contents

Keywords
International Ocean Discovery Program, IODP, Expedition 389, *MMA Valour*, Hawaiian Drowned Reefs, Earth climate system, Earth system feedbacks, Earth history tipping points, Site M0104, coral reef, volcanics, sea level, paleoclimate, central Pacific, reef health, Hawaiian geology, basalt, lava, carbonates, Hilo

Core descriptions

Supplementary material

References (RIS)

MS 389-111
Published 26 February 2025

Funded by ECORD, JAMSTEC, and NSF OCE1326927

1. Operations

The multipurpose vessel *MMA Valour* was used as the drilling platform throughout Expedition 389. At all Expedition 389 sites, dynamic positioning was used to provide accurate positions throughout operations and water depth was established using a Sound Velocity Profiler (SVP) placed on the top of the PROD5 drilling system. For more detail on acquisition methods, see **Introduction** in the Expedition 389 methods chapter (Webster et al., 2025a).

Summary operational information for Site M0104 is provided in Table **T1**. All times stated are in Hawaiian Standard Time (HST).

1.1. Hole M0104A

The *MMA Valour* arrived on location at 0000 h on 14 October 2023. PROD5 was deployed at 0842 h at a water depth of 347.0 m, and rotary coring in Hole M0104A began at 0945 h on 14 October. Rotary coring and casing continued throughout 15 October. Hole M0104A was terminated by mutual agreement between the Co-Chief Scientists and the European Consortium for Ocean Research Drilling Science Operator (ESO) at 0320 h on 16 October at 46.60 meters below seafloor (mbsf), and PROD5 was recovered to deck by 0448 h, when on-deck operations commenced and core barrels were extracted for curation. The decision to terminate the hole was made to move to Hole M0105A early enough for operations at one additional hole in the working area before a port call to the port of Hilo to address a medical issue with a drilling contractor.

A total of 22 cores were recovered from Hole M0104A with a total rotary cored depth of 46.39 m and a total recovered core length of 42.99 m (92.67% recovery).

Table T1. Hole summary, Site M0104. R = rotary coring mode. LAT = Lowest Astronomical Tide. **Download table in CSV format.**

Hole	Water depth (mbsf)	Date started (2023)	Date finished (2023)	Latitude	Longitude	Coring method	Total drilled depth (m)	Recovered length (m)	Core recovery (%)	Cores (*N*)	Notes
389-M0104A	347.0	14 Oct	16 Oct	19.870311°	–154.954000°	R	46.39	42.99	93	22	LAT water depth: 346.6 m. Borehole terminated as per client request.

2. Lithostratigraphy

Hole M0104A was recovered at 347 meters below sea level (mbsl) in the Hilo area. It spans 0.00 to 46.15 mbsf, and based on the main lithologic changes, discontinuity surfaces, and/or changes in physical properties, it is possible to identify five intervals (Figure **F1**):

- Interval 1 (0.00–0.80 mbsf) consists of biodetrital grainstone to rudstone and is bounded at its base by a major facies change and by a change in physical properties.
- Interval 2 (0.80–31.81 mbsf) consists predominantly of coralgal-microbial boundstone with occurrences of thin intervals of microbial-algal boundstone and algal boundstone. The base of this interval is marked by a sharp change in physical properties, specifically magnetic susceptibility, which gradually increases from approximately 20.00 to 31.81 mbsf and then drops abruptly to low values similar to those above this interval.
- The top of Interval 3 (31.81–39.87 mbsf) is a blackened, hardened, and bored surface. The interval is composed of consolidated biodetrital sediment and algal boundstone (with some coralgal boundstone intervals), and it is bounded at its base by a major facies change.
- The top of Interval 4 (39.87–43.39 mbsf) is marked by a heavily bioeroded surface. The interval comprises rhodoliths in the uppermost part, with coralgal boundstone, algal boundstone, and consolidated biodetrital sediment facies below. The base is marked by a coralgal boundstone accompanied by major changes in facies and some changes in physical properties.
- Interval 5 (43.39–46.15 mbsf) consists of coralgal boundstone, consolidated biodetrital sediment, and algal boundstone with higher magnetic susceptibility than Interval 4.

2.1. Hole M0104A

In Hole M0104A (Figure **F1**), consolidated biodetrital sediment (grainstone to rudstone) recovered from 0.00 to 0.80 mbsf (Figure **F2**) consists of robust branching to laminar *Porites* clasts, oyster shells, gastropods, and echinoid spines, with some coral clasts being encrusted with crustose coralline algae (CCA) that in turn are covered locally by microbialite crusts.

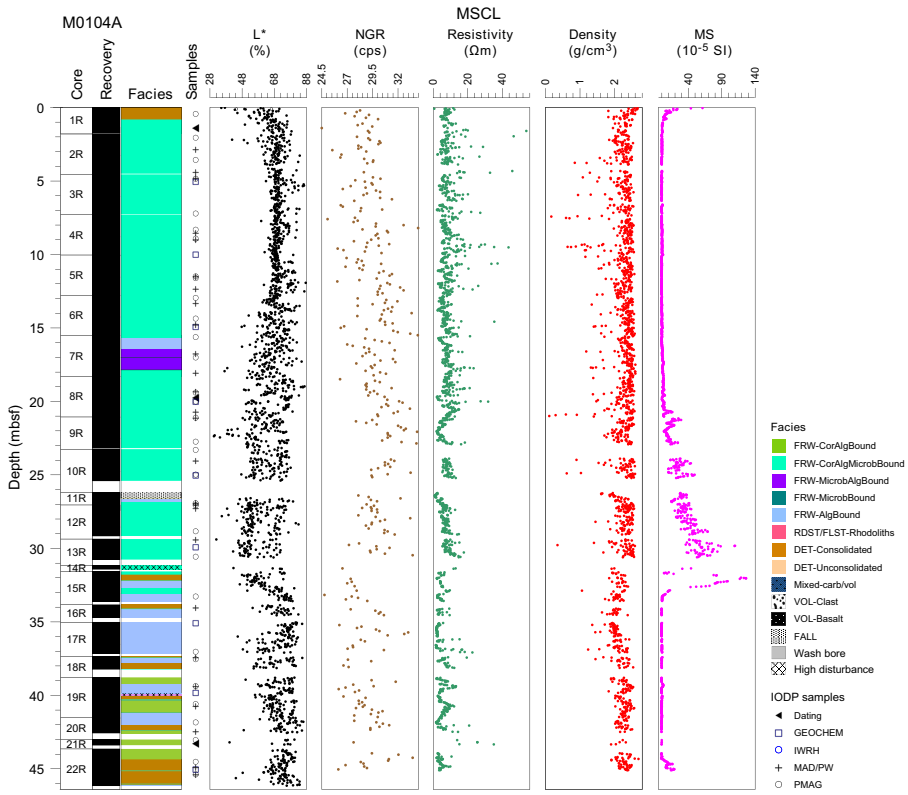

Figure F1. Lithostratigraphy and MSCL data, Hole M0104A. cps = counts per second, MS = magnetic susceptibility.

Coralgal-microbialite boundstone from 0.80 to 15.65 mbsf consists of branching, laminar, encrusting, and columnar *Porites* (e.g., 8.00 mbsf) (Figure **F3**) and locally encrusting *Cyphastrea* (Figure **F4**). In many cases, corals are encrusted with CCA incorporating vermetids and *Homotrema* (e.g., 10.88 mbsf), which are further encrusted with microbialite crusts (structureless, laminated, and dendritic; e.g., 10.35 mbsf) (Figure **F5**). In rare cases, corals show *Entobia* borings, most of which are infilled with sediments, commonly as geopetals. The boundstone also contains bivalves (e.g., oyster shells), gastropods, bryozoans, barnacles, a crab carapace, worm tubes, and cavities infilled with loose sediments. Algal boundstone from 15.65 to 16.40 mbsf consists of thick successions of

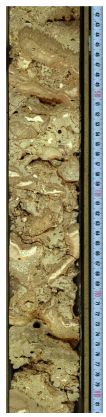

Figure F2. Lithology, Hole M0104A. Biodetrital grainstone (1R-1, 41–82 cm).

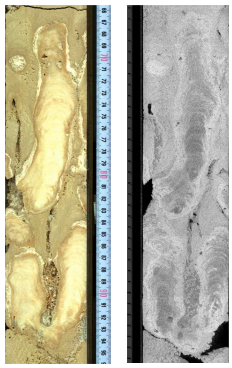

Figure F3. Lithology, Hole M0104A. Columnar *Porites* (4R-1, 66–96 cm). Left: high-resolution linescan image. Right: X-ray computed tomography scan image (orthogonal view 5°).

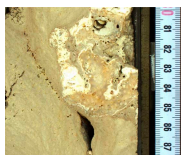

Figure F4. Lithology, Hole M0104A. *Cyphastrea* with CCA crust and capped by thick microbialite (5R-1, 80–87 cm).

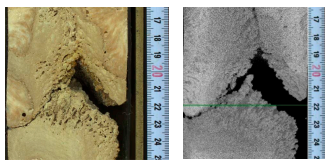

Figure F5. Lithology, Hole M0104A. Dendritic microbialite (3R-1, 17–24 cm) Left: high-resolution linescan image. Right: high-resolution computed tomography image.

CCA containing vermetids and *Homotrema*, coral clasts (encrusting *Cyphastrea* and branching to encrusting *Porites*), and thin microbialite crusts. Microbialite-algal boundstone from 16.40 to 17.86 mbsf contains abundant microbialite (structureless and laminated), CCA crusts (with vermetids), some encrusting to branching *Porites* clasts, and encrusting *Cyphastrea* clasts.

Coralgal boundstone from 17.86 to 25.40 mbsf consists of branching to columnar *Porites*, encrusting *Cyphastrea* (e.g., 18.26 mbsf), and *Pocillopora* that locally are encrusted with CCA (with vermetids and *Homotrema*) and microbialite (massive, laminated, and dendritic; e.g., 18.20 mbsf). Many corals are highly altered (e.g., 21.03 mbsf), and some show bioerosion with geopetal infills (e.g., 19.44 mbsf). Barnacles (e.g., 19.04 mbsf), gastropods, pectinid bivalves, and echinoid spines are present, and some parts of this core interval show irregular red-brown stains (e.g., 18.89 mbsf) (Figure **F6**). Fall-in material from 26.20 to 26.57 mbsf consists predominantly of gastropods, echinoid spines, bivalves, CCA and coral clasts, large benthic foraminifers (LBFs), and some volcaniclastics (e.g., 26.40 mbsf). From 26.57 to 26.82 mbsf, algal boundstone consists of thick CCA and fruticose coralline algae (FCA) with *Cyphastrea* clasts, *Homotrema*, and vermetids (e.g., 26.70 mbsf). Coralgal-microbialite boundstone from 26.82 to 31.81 mbsf contains *Porites* (branching, laminar, submassive, and massive) and encrusting *Cyphastrea*, both covered with CCA (with vermetids) and microbialite crusts (massive, laminated, and dendritic). The microbialites show several successive layers. Additionally, cavities in the framework contain serpulids (e.g., 28.97 mbsf), biodetrital sediment (echinoid spines and mollusk fragments), and volcaniclastic sediment.

Consolidated biodetrital sediment from 31.81 to 32.17 mbsf consists of reworked and bored CCA and FCA clasts, altered coral clasts, bryozoans, and bivalves in a fine-grained matrix with volcaniclastic grains (e.g., 32.00 mbsf). From 32.17 to 32.67 mbsf, algal boundstone contains abundant CCA and FCA (Figure **F7A**) with fine branching *Montipora* (e.g., 32.97 mbsf) (Figure **F7B**), serpulid tubes, bivalves, and gastropods. Coral boundstone from 32.67 to 33.06 mbsf contains *Cyphastrea* and *Porites* clasts (with borings by *Lithophaga*; e.g., 32.96 mbsf) that locally are encrusted with CCA (with *Homotrema*), FCA, and microbialite. Algal boundstone from 33.06 to 33.62 mbsf is composed predominantly of thick CCA crust with *Homotrema*, vermetids, and several *Cyphastrea* clasts. Biodetrital sediments and possible volcaniclastics are present in some pockets within the algal boundstone. Consolidated biodetrital sediment from 33.84 to 34.10 mbsf consists of CCA

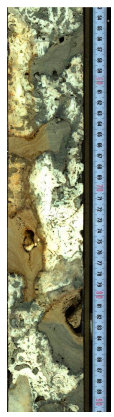

Figure F6. Lithology, Hole M0104A. Irregular red-brown stain (8R-1, 53–91 cm).

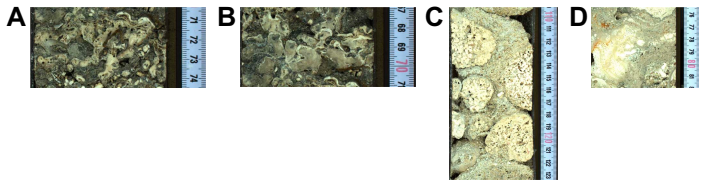

Figure F7. Lithologies, Hole M0104A. A. FCA (15R-1, 70–74 cm). B. Fine branching *Montipora* (15R-1, 67–70 cm). C. Rhodolith accumulation (19R-1, 109–123 cm). D. *Pocillopora* (19R-2, 77–81 cm).

and microbialite crust clasts, coral clasts, and echinoid spines. Algal boundstone from 34.10 to 36.90 mbsf contains thick CCA crusts with vermetids and *Homotrema*, thin microbialite crusts (laminated to dendritic), rare *Cyphastrea* clasts, and some unidentified coral clasts. Consolidated biodetrital sediment from 36.90 to 37.42 mbsf consists of bivalves, gastropods, echinoid spines, coral fragments, and reworked CCA and microbialite crust clasts. Algal boundstone from 37.42 to 37.77 mbsf is dominated by CCA with vermetids and a heavily bioeroded *Porites* clast. Consolidated biodetrital sediment (grainstone to rudstone) from 37.77 to 38.23 mbsf contains *Porites* fragments, gastropods, LBFs, echinoid spines, and CCA clasts with microbialite crusts. From 38.77 to 39.20 mbsf, coralgal boundstone is formed of massive *Porites* with CCA, with some framework cavities containing coarse bioclastic sediments (with bivalves and gastropods). Algal boundstone from 39.20 to 39.87 mbsf consists predominantly of CCA crusts with some FCA encrusted with thin microbialite crusts. The CCA crusts also contain vermetids, *Homotrema*, and *Cyphastrea* clasts, and some cavities are filled with sediment.

A rhodolith accumulation recovered from 39.87 to 39.99 mbsf (Figure **F7C**) consists of well-developed praline-type rhodoliths embedded in unconsolidated bioclastic sediment. From 39.99 to 40.35 mbsf, consolidated biodetrital sediment contains bivalves, gastropods, coral and CCA debris, and LBFs. Coralgal boundstone from 40.35 to 41.09 mbsf consists of *Cyphastrea* and branching *Pocillopora* encrusted with CCA (Figure **F7D**), with bioclastic sediments in cavities. Consolidated biodetrital sediment (41.09–41.15 mbsf) overlies algal boundstone (41.15–41.97 mbsf) composed predominantly of CCA with vermetids and *Homotrema*, rhodoliths (with *Porites* nuclei), and a few encrusting and branching *Pocillopora*. Consolidated biodetrital sediment from 41.97 to 42.37 mbsf has a predominantly bioclastic matrix with rare CCA and branching *Porites* clasts. Coralgal boundstone from 42.37 to 43.39 mbsf consists of submassive *Porites* with thin CCA crusts. From 43.39 to 44.10 mbsf, coralgal boundstone consists of submassive *Porites* with CCA crusts and rare gastropods, bivalves, and echinoid spines.

Consolidated biodetrital sediment from 44.10 to 46.02 mbsf consists of FCA clasts, barnacles, echinoid spines, *Porites* and *Cyphastrea* clasts, and rhodoliths. Algal boundstone composed predominantly of CCA crust forms the base of the core from 46.02 to 46.15 mbsf.

3. Physical properties

Physical properties data for Site M0104 are shown in Table **T2** in the Site M0096 chapter (Webster et al., 2025b).

3.1. Hole M0104A

A total of 42.77 m of core of Hole M0104A was scanned with the multisensor core logger (MSCL), and the core exhibited only minor drilling-induced disturbance, with over 85% of the acquired data passing QA/QC (see Table **T10** in the Expedition 389 methods chapter [Webster et al., 2025a]). A total of 26 discrete samples were taken for *P*-wave velocity and moisture and density (MAD) measurements. Digital linescans, color reflectance, and hyperspectral imaging were acquired on all cores.

3.1.1. Density and porosity

Data for density and porosity measurements are presented in Figures **F1** and **F8**. MSCL bulk density values range 0.11–2.69 g/cm^3. Low densities (<1 g/cm^3) represent natural vugs (rather than drilling-induced damages, which have been cleaned up in all MSCL data sets). A total of 26 discrete samples were analyzed for MAD, giving bulk density values in the range of 2.09–2.52 g/cm^3. Porosity values range 13.4%–40.4% (Figure **F8**), and grain density values range 2.723–2.850 g/cm^3. There is a clear relationship between the two bulk density measurements (MSCL and discrete).

3.1.2. *P*-wave velocity

MSCL *P*-wave velocity measurements yielded no data. A total of 26 samples were measured using the discrete *P*-wave logger. Dry measurement values range 3148–5323 m/s (Figure **F9**). *P*-wave velocity recorded for the same samples after resaturation range 3384–6076 m/s.

3.1.3. Thermal conductivity

Thermal conductivity was collected on five cores (see Table **T11** in the Expedition 389 methods chapter [Webster et al., 2025a]) and ranges 1.126–1.529 W/(m·K).

3.1.4. Magnetic susceptibility

MSCL magnetic susceptibility data range -0.74×10^{-5} to 126.30×10^{-5} SI (Figure **F1**), with the majority of magnetic susceptibility values close to 8.68×10^{-5} SI. From about 21 to 32 mbsf, magnetic susceptibility values gradually increase downhole from ~2×10^{-5} SI to the maximum value for the hole, 126.30×10^{-5} SI. Just below ~32 mbsf, a sharp change to negative values occurs, followed by a slight increase to ~19×10^{-5} SI near the base of the hole below ~44 mbsf. The variations in magnetic susceptibility appear to correlate with a change in carbonate facies at similar depths from coralgal-microbialite boundstone on top to algal boundstone below (see **Lithostratigraphy**).

3.1.5. Electrical resistivity

MSCL noncontact resistivity measurements range 0.98–53.97 Ωm (Figure **F1**). No downhole trends are apparent.

3.1.6. Natural gamma radiation

MSCL natural gamma radiation (NGR) measurements range 25–34 counts/s (Figure **F1**) and show no apparent downhole trend.

3.1.7. Digital linescans, color reflectance, and hyperspectral imaging

All cores from Hole M0104A were digitally scanned, measured for color reflectance (where appropriate), and imaged with the hyperspectral scanner (see HYPERSPECTRAL in **Supplementary material**). Color reflectance L* values vary between 30.51% and 87.52%, a* varies between –1.34

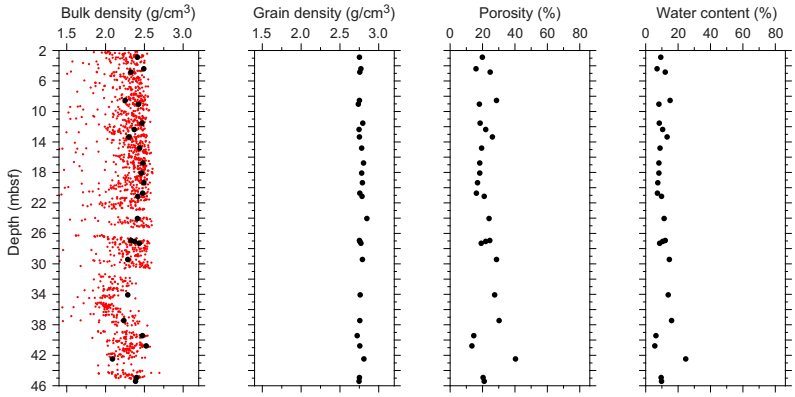

Figure F8. Physical properties, Hole M0104A. Black = discrete samples, red = MSCL.

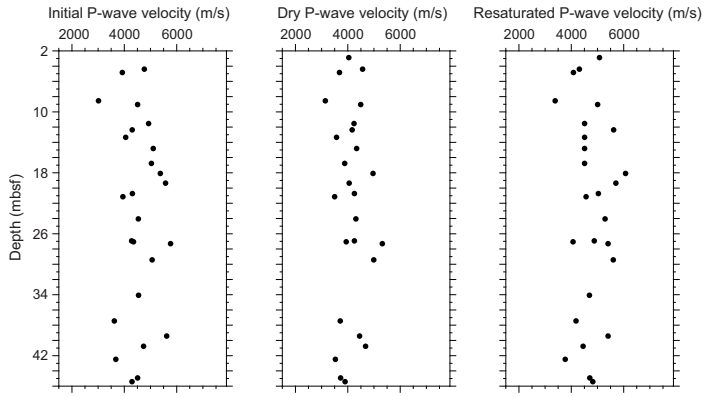

Figure F9. Initial, dry, and resaturated *P*-wave velocities measured on discrete samples, Hole M0104A.

and 9.19, b* varies between –1.13 and 32.58, and a*/b* varies between –0.27 and 0.42 (Figure **F1**). A downhole trend begins at 13 mbsf from higher average L* values above to lower and more variability values below to ~32 mbsf. Below ~32 mbsf, L* values are generally higher and have less variability than in the interval above this depth, consistent with a major change in lithology (see **Lithostratigraphy**).

4. Geochemistry

4.1. Interstitial water

No interstitial water samples were collected from Site M0104.

4.2. Surface seawater

One surface seawater sample was collected from Site M0104 using a Niskin bottle deployed from the side of the vessel (see Figure **F22** in the Expedition 389 methods chapter [Webster et al., 2025a]). The salinity, pH, alkalinity, ammonium, and major element chemistry measured for this sample are consistent with the other surface seawater samples taken during Expedition 389 and align with the expected values for conservative elements in seawater (see Tables **T15** and **T17** in the Expedition 389 methods chapter [Webster et al., 2025a]).

4.3. Bulk sediment and rocks

Nine bulk sediment samples were taken from Site M0104 (Hole M0104A) (Figure **F1**) and analyzed for mineralogy and elemental composition. Samples were composed of mixed microbialite, coralline algae, small fragments of coral, mixtures of these, and some unconsolidated sediment facies in sections classified as coralgal-microbialite boundstone and algal boundstone (see Figure **F10** in the Expedition 389 methods chapter [Webster et al., 2025a]).

4.4. Mineralogy

Samples from Hole M0104A are composed of almost purely carbonate minerals dominated by high-Mg calcite (Table **T2**). Only one sample with mixed microbialite and sediment (Sample 22R-1, 140.5–142.5 cm; 45.05 mbsf) contains small amounts of silicate minerals identified as pyroxenes (3%) and Fe oxides and Fe hydroxides (2%).

4.5. Elemental abundances

The concentrations of major elements in the bulk sediment and rock samples from Hole M0104A are similar (Table **T3**) and reflect the dominance of carbonate minerals. Below 14.92 mbsf, samples composed of microbialite often have higher concentrations of elements associated with terrigenous sediments (e.g., Fe, Mn, and Ti). The one coralline algae sample analyzed (17R-1, 7–10 cm; 35.09 mbsf) is very pure carbonate without no detectable amounts of Fe, Mn, and Ti.

4.6. Carbon content

The results and lithologies for total organic carbon (TOC) and total inorganic carbon (TIC) from Hole M0104A are presented in Table **T4**. TOC content ranges 0.14%–0.24%, total carbon (TC) content ranges between 11.1%–11.9%, and TIC ranges 10.95%–11.73%, which equates to $CaCO_3$ contents of 91%–98% (for CaCO percent calculation, see GEOCHEM in **Supplementary material**).

Table T2. HighScore X-ray diffraction (XRD) mineral abundances, Site M0104. **Download table in CSV format.**

Table T3. Solid-phase elemental abundances, Site M0104. **Download table in CSV format.**

Table T4. TOC, TIC, and TC, Site M0104. **Download table in CSV format.**

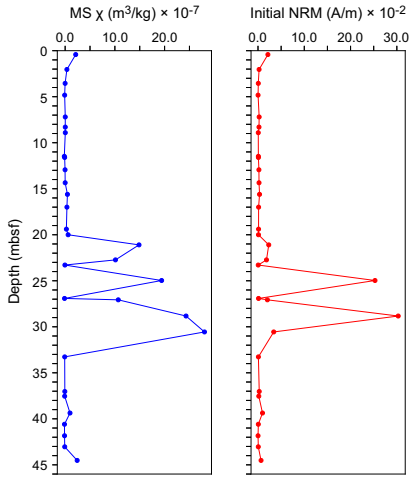

Figure F10. Magnetic susceptibility (MS) and NRM, Hole M0104A.

5. Paleomagnetism

A total of 32 plug samples were obtained from Hole M0104A. Measurements of low-field and mass-specific magnetic susceptibility (χ) were carried out for all samples. Natural remanent magnetization (NRM) was measured for all samples, as well as remanence following stepwise alternating field (AF) demagnetization up to a peak AF of 20 mT. For further details, see **Paleomagnetism** in the Expedition 389 methods chapter (Webster et al., 2025a).

5.1. Hole M0104A

A total of 32 carbonate samples were taken from Hole M0104A (Figure **F10**). Some of the χ and initial NRM values were relatively high because the samples likely included some volcanic material. The χ values range -0.17×10^{-7} to 28.0×10^{-7} m^3/kg with an arithmetic mean of 3.59×10^{-7} m^3/kg. The χ values peak and fluctuate between 20.01 mbsf (Sample 8R-2, 23–25 cm) and 33.27 mbsf (Sample 15R-2, 21–23 cm). The initial NRM intensity ranges 0.010×10^{-2} to 30.3×10^{-2} A/m with an arithmetic mean of 2.27×10^{-2} A/m. NRM values fluctuate between 23.30 mbsf (Sample 10R-1, 4–6 cm) and 30.58 mbsf (Sample 13R-1, 120–122.5 cm). These data appear to be consistent with an increasing trend in the MCSL magnetic susceptibility data over the same depths (20.01–33.28 mbsf) (Figure **F1**) (see **Physical properties**).

6. Geochronology

A total of three U-Th dates were obtained from corals from Hole M0104A (see Tables **T21** and **T22** in the Expedition 389 methods chapter [Webster et al., 2025a]). None of the dates for Site M0104 were rejected, and dates from these three samples (1R-2, 3–7 cm; 8R-1, 146–148 cm; and 21R-1, 29–30 cm) range ~130–159 ky BP with no stratigraphic age reversals. These dates are consistent with the estimated age of the H2 terrace (Ludwig et al., 1991; Webster et al., 2009).

References

Ludwig, K.R., Szabo, B.J., Moore, J.G., and Simmons, K.R., 1991. Crustal subsidence rate off Hawaii determined from $^{234}U/^{238}U$ ages of drowned coral reefs. Geology, 19(2):171–174. **https://doi.org/10.1130/0091-7613(1991)019<0171:CSROHD>2.3.CO;2**

Webster, J.M., Braga, J.C., Clague, D.A., Gallup, C., Hein, J.R., Potts, D.C., Renema, W., Riding, R., Riker-Coleman, K., Silver, E., and Wallace, L.M., 2009. Coral reef evolution on rapidly subsiding margins. Global and Planetary Change, 66(1–2):129–148. **https://doi.org/10.1016/j.gloplacha.2008.07.010**

Webster, J.M., Ravelo, A.C., Grant, H.L.J., and the Expedition 389 Scientists, 2025. Supplementary material, **https://doi.org/10.14379/iodp.proc.389supp.2025**. In Webster, J.M., Ravelo, A.C., Grant, H.L.J., and the Expedi-

tion 389 Scientists, Hawaiian Drowned Reefs. Proceedings of the International Ocean Discovery Program, 389: College Station, TX (International Ocean Discovery Program).

Webster, J.M., Ravelo, A.C., Grant, H.L.J., Rydzy, M., Stewart, M., Allison, N., Asami, R., Boston, B., Braga, J.C., Brenner, L., Chen, X., Chutcharavan, P., Dutton, A., Felis, T., Fukuyo, N., Gischler, E., Greve, S., Hagen, A., Hamon, Y., Hathorne, E., Humblet, M., Jorry, S., Khanna, P., Le Ber, E., McGregor, H., Mortlock, R., Nohl, T., Potts, D., Prohaska, A., Prouty, N., Renema, W., Rubin, K.H., Westphal, H., and Yokoyama, Y., 2025a. Expedition 389 methods. In Webster, J.M., Ravelo, A.C., Grant, H.L.J., and the Expedition 389 Scientists, Hawaiian Drowned Reefs. Proceedings of the International Ocean Discovery Program, 389: College Station, TX (International Ocean Discovery Program). **https://doi.org/10.14379/iodp.proc.389.102.2025**

Webster, J.M., Ravelo, A.C., Grant, H.L.J., Rydzy, M., Stewart, M., Allison, N., Asami, R., Boston, B., Braga, J.C., Brenner, L., Chen, X., Chutcharavan, P., Dutton, A., Felis, T., Fukuyo, N., Gischler, E., Greve, S., Hagen, A., Hamon, Y., Hathorne, E., Humblet, M., Jorry, S., Khanna, P., Le Ber, E., McGregor, H., Mortlock, R., Nohl, T., Potts, D., Prohaska, A., Prouty, N., Renema, W., Rubin, K.H., Westphal, H., and Yokoyama, Y., 2025b. Site M0096. In Webster, J.M., Ravelo, A.C., Grant, H.L.J., and the Expedition 389 Scientists, Hawaiian Drowned Reefs. Proceedings of the International Ocean Discovery Program, 389: College Station, TX (International Ocean Discovery Program). **https://doi.org/10.14379/iodp.proc.389.103.2025**